

THE MECHANICAL PROPERTIES OF ULTRAFINE-GRAINED METALS AT ELEVATED TEMPERATURES

Roberto B. Figueiredo¹, Megumi Kawasaki¹ and Terence G. Langdon^{1,2}

¹Departments of Aerospace & Mechanical Engineering and Materials Science, University of Southern California, Los Angeles, CA 90089-1453, USA

²Materials Research Group, School of Engineering Sciences, University of Southampton, Southampton SO17 1BJ, UK

Received: September 03, 2008

Abstract. Ultrafine-grained materials, having grain sizes in the submicrometer or nanometer range, may be readily produced by processing bulk solids through the application of severe plastic deformation (SPD) and this leads to the possibility of revealing different flow mechanisms when these materials are tested at elevated temperatures. Experiments show the two-phase Zn-22% Al alloy and various magnesium alloys exhibit excellent superplastic properties after processing by SPD whereas it is not possible to reveal different creep mechanisms in high-purity aluminum because the ultrafine grains are unstable at high temperatures.

1. INTRODUCTION

An important development in the last twenty years was the recognition that the processing of metals through the application of severe plastic deformation (SPD) provides an opportunity for achieving exceptional grain refinement in crystalline bulk solids such that the grains are reduced to within the submicrometer or even the nanometer range [1]. Several different SPD processing techniques are now available but most attention is generally devoted to Equal-Channel Angular Pressing (ECAP) [2] and High-Pressure Torsion (HPT) [3]. In both of these procedures, exceptionally high strains are introduced without incurring any significant change in the overall dimensions of the samples [4]. Thus, SPD processing differs in a very significant way from the more conventional industrial processing techniques such as extrusion, rolling and drawing.

The introduction of significant grain refinement in bulk metals opens the possibility of achieving high tensile ductilities, including superplastic elongations, when these materials are tested in ten-

sion at elevated temperatures. For example, it is well established that superplasticity requires both a high testing temperature, typically above $\sim 0.5 T_m$ where T_m is the absolute melting temperature of the material, and a grain size less than $\sim 10 \mu\text{m}$ [5]. Conventional superplastic metals usually have grain sizes of $\sim 2 - 5 \mu\text{m}$ but materials processed by SPD have even smaller grain sizes lying in the submicrometer range. As a consequence of this exceptional grain refinement, it is probable that SPD processing may produce materials that can be utilized in superplastic forming operations, where this type of forming is now well established for the fabrication of a wide range of commercial products for use in the aerospace, automotive and other sectors [6]. It is important to note that the occurrence of superplastic behavior after SPD processing was first demonstrated in a very early report where an elongation of 800% was achieved in an Al-4% Cu-0.5% Zr alloy after processing by HPT [7]. More recently, a superplastic forming capability was demonstrated directly for an Al-3% Mg-0.2% Sc alloy after processing by ECAP [8]. These and other results there-

Corresponding author: Terence G. Langdon, e-mail: langdon@usc.edu

fore confirm the potential for developing superplastic ductilities in the ultrafine-grained materials processed by SPD [9,10].

The objective of this paper is to examine the high temperature mechanical properties of materials processed using ECAP. Accordingly, the following section describes the results obtained in the creep testing of high-purity aluminum, section 3 summarizes the results from the testing of a Zn-22% Al eutectoid alloy which is taken as a representative two-phase alloy and section 4 describes the results of the tensile testing of some representative magnesium alloys at elevated temperatures.

2. CREEP BEHAVIOR OF PURE ALUMINUM PROCESSED BY ECAP

Processing by ECAP was conducted with high-purity (99.99%) aluminum at room temperature for a total of 4 passes using route B_c where the sample is rotated by 90° in the same direction between each pass [11,12]. Since the ECAP die had a channel angle of 90°, the imposed strain was ~1 on each separate pass [13] and the total imposed strain was ~4 after pressing through 4 passes. As demonstrated in earlier reports [14-17], the initial grain size of $d \approx 1$ mm was refined to $d \approx 1.3$ μm in pure Al through processing by ECAP and these ultrafine grains were reasonably equiaxed.

All as-pressed samples were tested under tensile creep conditions of constant stress. For each specimen, the tensile axis was oriented parallel to the pressing direction. The creep specimens were tested at a temperature of 473K using selected constant stresses within the range from 10 to 50 MPa. Each creep test was terminated before fracture and a detailed investigation was then focused on the creep behavior occurring within the steady-state region.

All of the experimental data were plotted in the form of strain versus time ($\epsilon-t$), strain rate versus time ($\dot{\epsilon}-t$) and strain rate versus strain ($\dot{\epsilon}-\epsilon$) where these plots are shown in Figs. 1-3, respectively. For comparison purposes, creep testing was also conducted at 473K using an unpressed pure Al sample at a constant stress of 20 MPa and this result is included in Figs. 1-3. The conditions of the Al samples used in the tensile creep tests are summarized in Table 1 which shows the specimen elongations and the creep testing times up to the point where each test was terminated without failure [18].

From inspection of Fig. 1, the as-pressed samples exhibit normal creep curves with a short primary creep stage and a reasonable steady-state

Table 1. Specimen elongations and testing times for tensile creep tests at 473K of pure Al unpressed and after processing by ECAP for 4 passes [18].

Stress (MPa)	As-pressed (4p, RT, B _c) (initial $d = 1.3$ μm): total elongation and time	Unpressed (initial $d = 1$ mm): total elongation and time
10	9% (337 h)	–
15	10% (69 h)	–
20	13% (81 h)	20% (12 h)
25	11% (4 h)	–
30	15% (7 h)	–
40	15% (0.5 h)	–
50	10% (0.15 h)	–

region. The transition of creep rates from the primary stage to the steady-state stage is illustrated clearly in Figs. 2 and 3 for all creep conditions [18].

Detailed evaluation of Figs. 1-3 shows that the steady-state strain rate of the unpressed sample with a coarse grain size is almost one order of magnitude faster than for the as-pressed sample having an ultrafine grain size tested under the same conditions of 20 MPa at 473K. Similar results were reported also in earlier experiments on the creep testing of as-pressed pure Al [19-23]. More detailed information on the present creep results for pure Al was presented recently with information of the evolution of the creep texture [18]. However, it should be noted that creep data are available to date for only a limited number of materials processed by ECAP: Al alloys [23,24], high-purity Cu [25-28] and commercial-purity Ti [28].

Fig. 4 displays a logarithmic plot of the steady-state creep rate versus the applied stress for both the as-pressed pure Al samples using a range of applied stresses and the unpressed sample using an applied stress of 20 MPa [18]. The stress exponent, n , as given by the slope of the plot was measured as ~5 for pure Al tested in creep at 473K and this value is consistent with earlier reports for the creep testing of pure Al after ECAP where $n \approx 4.8$ in compression [20] and $n \approx 5.7$ in tension [22] at 473K.

Detail inspection of Fig. 4 confirms the lower creep rate in the as-pressed material compared to the unpressed Al at an applied stress of 20 MPa

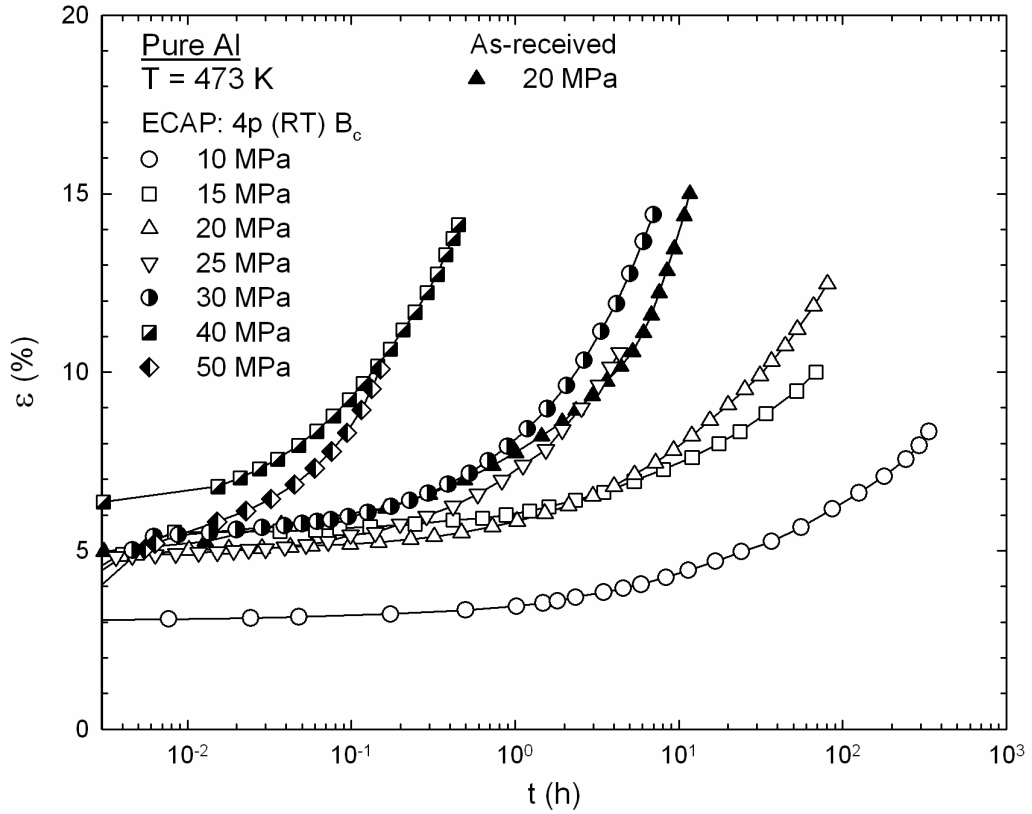


Fig. 1. Strain versus testing time for the as-pressed and unpressed pure Al tested at a temperature of 473K.

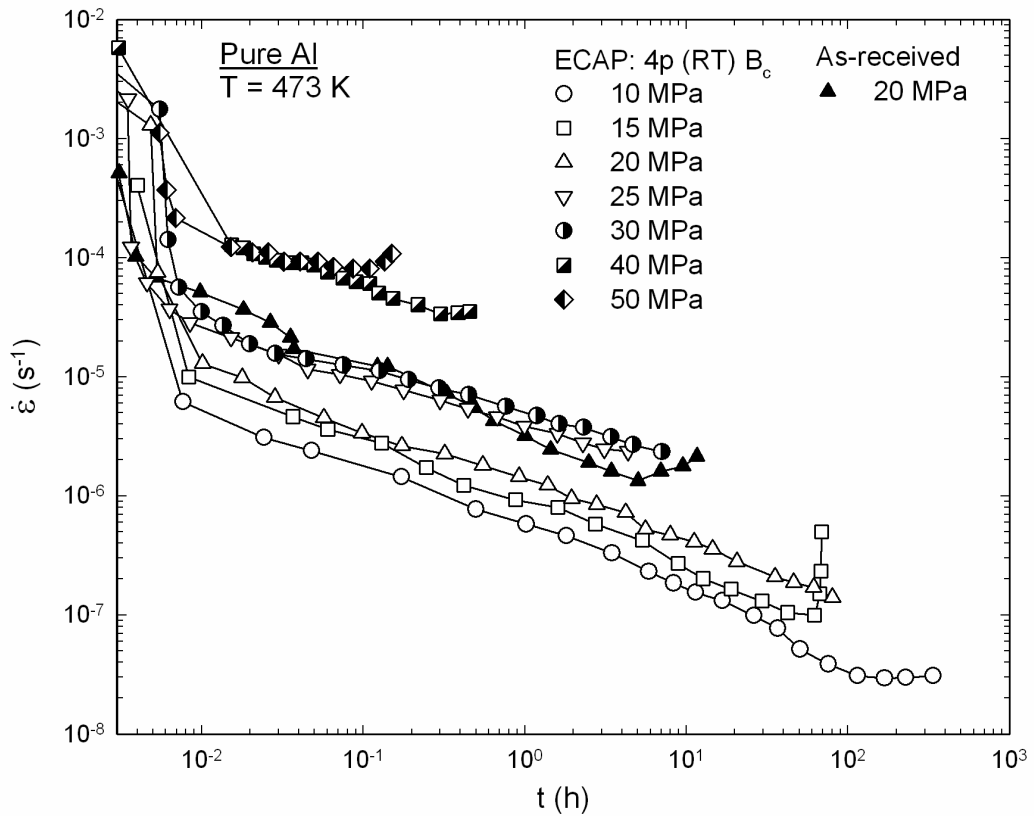


Fig. 2. Strain rate versus testing time for the as-pressed and unpressed pure Al tested at a temperature of 473K.

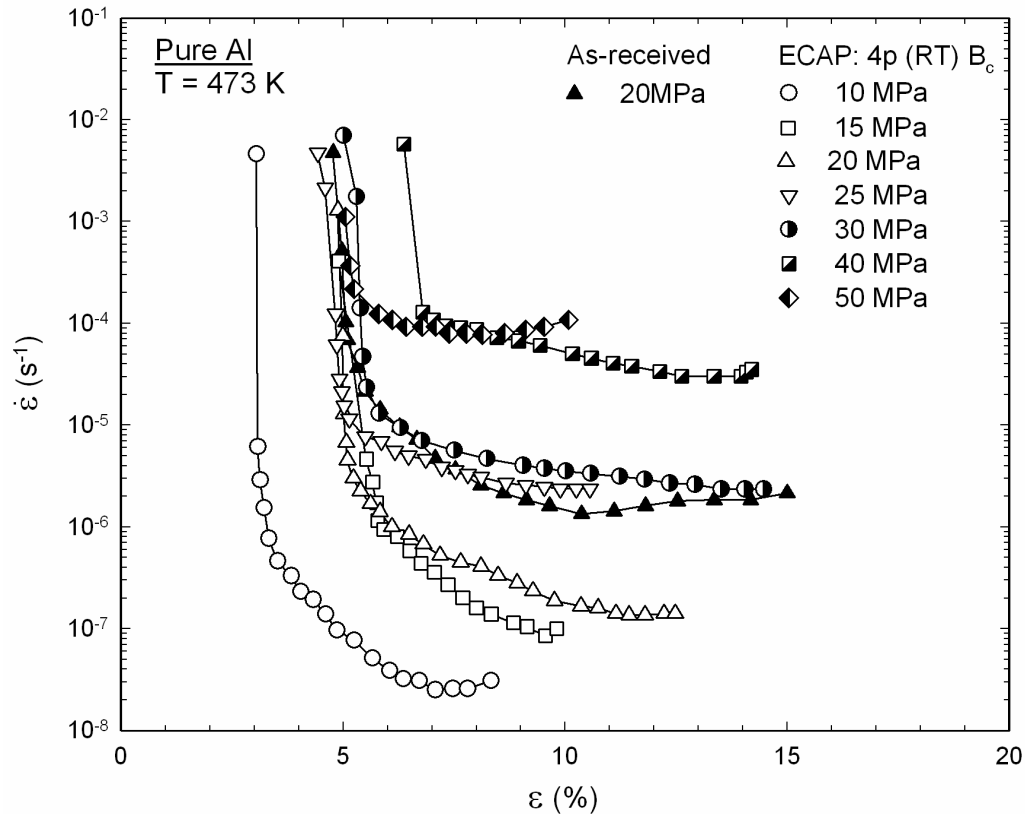


Fig. 3. Strain rate versus strain for creep tests of the as-pressed pure Al over a range of stresses and the unpressed pure Al tested at 20 MPa at a temperature of 473K.

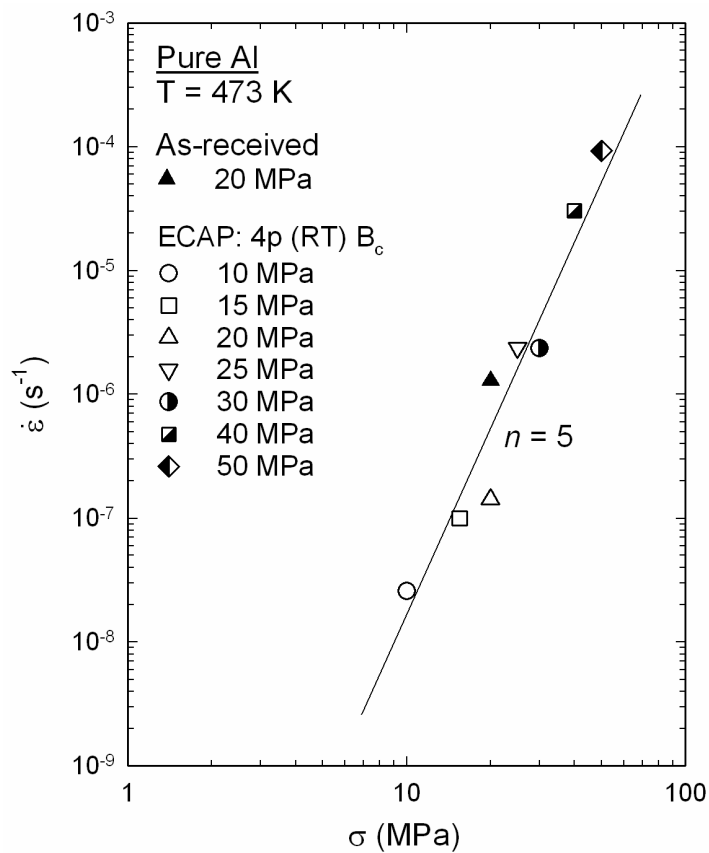


Fig. 4. Logarithmic plot of minimum creep rate versus applied stress for an unpressed specimen tested at a temperature of 473K under a constant stress of 20 MPa and for a number of specimens processed by ECAP and subsequently creep tested at different levels of constant stress at 473K (data from [18]).

and this result is not supported by the general relationship of the steady-state creep rate in terms of grain size. Moreover, the present results are not consistent with earlier results showing there is no dependence on grain size in the dislocation creep region [29]. Therefore, the trend of slower creep rates in the as-pressed material cannot be a consequence of any significant change in the rate-controlling process in creep behavior. It is probable that the result reflects a significant difference in the microstructural characteristics of the as-pressed materials including the high dislocation densities introduced during ECAP [30,31], the presence of non-equilibrium grain boundaries having an excess of extrinsic dislocations [32] and the lower fraction of high-angle grain boundaries by comparison with conventional materials [17].

In general, the steady-state creep rate in polycrystalline materials is given by a relationship of the form [33,34]:

$$\dot{\epsilon} = \frac{ADGb}{kT} \left(\frac{\mathbf{b}}{d} \right)^p \left(\frac{\sigma}{G} \right)^n, \quad (1)$$

where $\dot{\epsilon}$ is the steady-state strain rate, A is a dimensionless constant, G is the shear modulus, \mathbf{b} is the Burgers vector, k is Boltzmann's constant, D is the appropriate diffusion constant [given by $D_0 \exp(-Q/RT)$ where D_0 is a frequency factor, Q is the activation energy and R is the gas constant], σ is the applied stress, and n and p are the exponents of the stress and the inverse grain size, respectively.

The two types of material shown in Fig. 4 have different grain sizes of $\sim 1.3 \mu\text{m}$ in the pressed aluminum and $\sim 1 \text{mm}$ in the unpressed material. For the ultrafine grain sizes produced by ECAP, it is expected that Nabarro-Herring [35,36] or Coble [37] diffusion creep may make important contributions to the overall deformation. Eq. (1) can describe both of these flow mechanisms with values of $A = 28$, $n = 1$, $p = 2$ and $D = D_l$ for Nabarro-Herring creep where D_l is the coefficient for lattice self-diffusion and values of $A = 66.8 \delta/\mathbf{b}$, $n = 1$, $p = 3$ and $D = D_{gb}$ for Coble creep where δ is the grain boundary width and D_{gb} is the coefficient for grain boundary diffusion. Performing a calculation with values of $D_l = 1.86 \cdot 10^{-4} \exp(-143,400/RT) \text{ m}^2 \text{ s}^{-1}$ and $D_{gb} = 1.86 \cdot 10^{-4} \exp(-86,000/RT) \text{ m}^2 \text{ s}^{-1}$ for pure aluminum with $\mathbf{b} = 2.86 \cdot 10^{-10} \text{ m}$ and $\delta = 2\mathbf{b} = 5.72 \cdot 10^{-10} \text{ m}$ [38] and $G = 2.54 \cdot 10^4 (1 - 0.5\{(T - 300)/933\}) \text{ MPa}$ [39], the predicted strain rates for Nabarro-Herring creep and Coble creep at 10 MPa and 473K are estimated as

$\sim 1.6 \cdot 10^{-8} \text{ s}^{-1}$ and $\sim 1.8 \cdot 10^{-5} \text{ s}^{-1}$, respectively. It is apparent that Nabarro-Herring creep occurs too slowly to make any significant contribution to the flow process but Coble creep appears to be a viable deformation mechanism whereas there is no evidence for any transition at lower stresses to a region having $n = 1$.

This inconsistency is readily explained by the inherent microstructural instability in high-purity materials. Since the ultrafine grains in the as-pressed high-purity Al contain no precipitates, unlike many of the commercial aluminum-based alloys, those small grains are not sufficiently stable at elevated temperature. It was noted in an earlier report that the ultrafine grains of high purity Al grow rapidly from $\sim 1 \mu\text{m}$ to $\sim 10\text{-}12 \mu\text{m}$ in the early stages of annealing at 473K [23]. Thus, it is expected that, since the creep rate varies inversely with grain size raised to $p = 3$ in Coble diffusion creep, the predicted creep rate is probably reduced to $\sim 1.8 \cdot 10^{-8} \text{ s}^{-1}$. These results lead to the conclusion that the creep behavior of pure Al processed by ECAP is similar to that of conventional materials with coarse grains because of the difficulties in retaining ultrafine grain sizes at these elevated temperatures. The results demonstrate also that the instabilities in the ultrafine grains in high-purity materials such as aluminum will effectively prevent the occurrence of superplastic flow in these materials.

3. SUPERPLASTICITY IN A TWO-PHASE Zn-22% Al EUTECTOID ALLOY

Optimal superplastic alloys tend to be either two-phase eutectic or eutectoid alloys or alloys containing a fine dispersion of a second phase to avoid grain growth during high temperature deformation. When a superplastic material is deformed in tension, the following relationship relates the stress to strain rate through the strain rate sensitivity, m :

$$\sigma = K\dot{\epsilon}^m, \quad (2)$$

where K is a constant which depends on testing temperature and grain size. Accordingly, the relation between σ and $\dot{\epsilon}$ can reveal the value of m from the inclination of the slope when Eq. (2) is plotted in a logarithmic plot. As was noted earlier [40], superplastic metals often show a sigmoidal curve in this type of plot with a high strain rate sensitivity of $m \approx 0.5$ at intermediate strain rates. A value of $m > 0.3$ is generally recognized for the occurrence of superplasticity and the region of optimal strain rates is

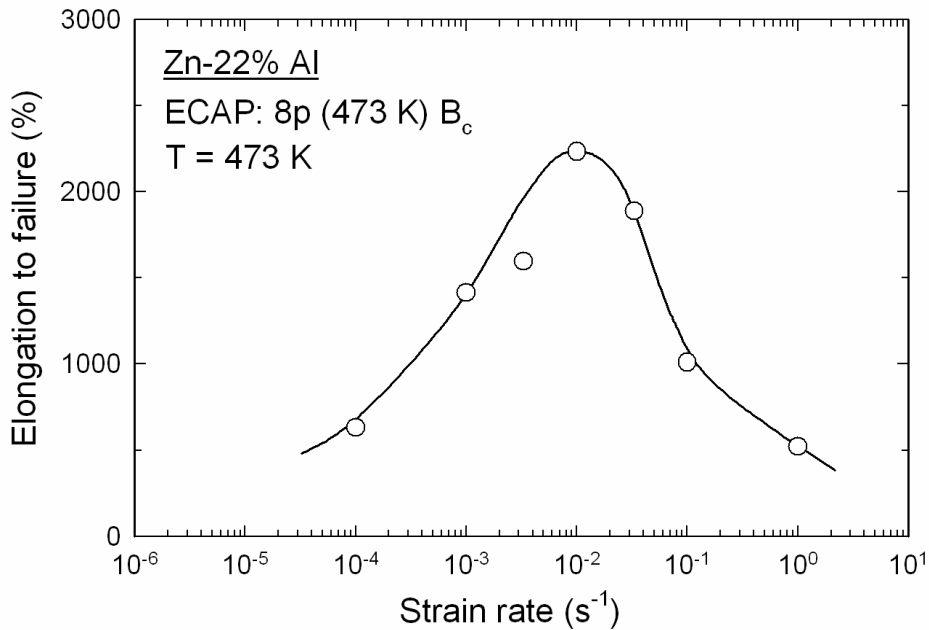


Fig. 5. Variation of elongation to failure versus strain rate for the as-pressed Zn-22% Al alloy tested at 473K (data from [43]).

termed region II. In practice, there are decreases in the strain rate sensitivity at both lower strain rates in region I and at faster strain rates in region III. Although this type of behavior is now a recognized general characteristic of superplastic metals, it was first documented in experiments conducted on the Zn-22% Al eutectoid alloy [41].

To provide more comprehensive information of superplasticity in ultrafine-grained alloys, processing by ECAP was conducted with the Zn-22% Al eutectoid alloy where the alloy contained the following impurities in ppm: Cr <10, Cu 20, Fe 70, Mg <10, Mn <10, and Si 70 [42,43]. It is well known that this alloy has a binary microstructure of Al-rich and Zn-rich phases and in the present experiments the average linear intercept grain size was $\sim 1.8 \mu\text{m}$.

All samples were pressed for a total of 8 passes at 473K using route B_c leading to an imposed strain equal to ~ 8 for each sample. The longitudinal grain size immediately after pressing was measured as $\bar{L} \approx 0.8 \mu\text{m}$ [44].

After pressing, tensile testing was carried out to observe the tensile properties of the Zn-Al alloy processed by ECAP. One set of tensile specimens was pulled to failure at several different strain rates from $1.0 \cdot 10^{-4}$ to 1.0 s^{-1} at 473K and investigations were made to determine the nature of the relationship between σ and $\dot{\epsilon}$ in the as-pressed Zn-Al alloy. It should be noted that a mean linear intercept grain

size of $\bar{L} \approx 0.9 \mu\text{m}$ was measured in the sample immediately before tensile testing [45].

The tensile testing results are recorded in a plot of the variation of the elongation to failure versus strain rate as shown in Fig. 5 [43]. The highest elongation of 2230% was observed at a strain rate of $1.0 \cdot 10^{-2} \text{ s}^{-1}$ and this confirms that the Zn-Al alloy exhibits high strain rate superplasticity after ECAP. From this plot, three distinct regimes of strain rate are delineated where the superplastic elongations of $>1500\%$ can be classified into region II and the slower and faster strain rates correspond to regions I and III, respectively.

In order to evaluate the rate-controlling process, Fig. 6 shows a plot of strain rate versus stress for the samples recorded in Fig. 5. From a theoretical analysis, the strain rate for superplastic deformation is given by the following relationship [46]:

$$\dot{\epsilon}_{sp} = \frac{10D_{gb}Gb}{kT} \left(\frac{b}{d_s} \right)^2 \left(\frac{\sigma}{G} \right)^2, \quad (3)$$

where $\dot{\epsilon}_{sp}$ is the strain rate for superplasticity and d_s is the average spatial grain size. This relationship was used to give the predicted line for grain boundary sliding using a spatial grain size of $d_s = 1.74 \cdot 0.9 = 1.6 \mu\text{m}$. This predicted superplastic flow behavior is consistent with the experimental results to within less than one order of magnitude of strain

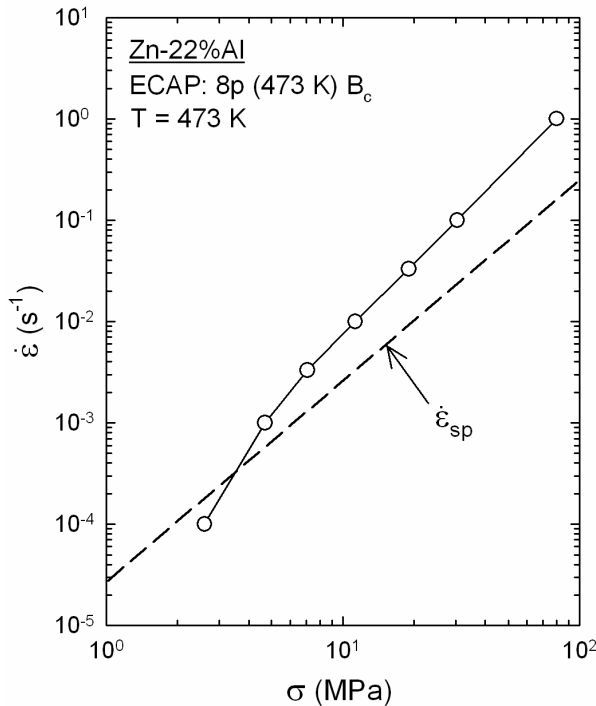


Fig. 6. Variation of flow stress with strain rate for as-pressed Zn-22% Al alloy tested at 473K [data from 43]: the broken line shows the prediction for superplastic flow at 473K (data from [46]).

rate, thereby confirming the validity of the conventional relationship for superplastic flow when extended to materials with submicrometer grain sizes.

4. THE DEVELOPMENT OF SUPERPLASTICITY IN MAGNESIUM ALLOYS

The high temperature behavior of metallic materials depends on the controlling deformation mechanism. Dislocation slip and diffusion mechanisms may operate depending upon the material grain structure, the temperature and the magnitude of the imposed stress. Processing magnesium alloys through ECAP leads to the development of reasonably fine microstructures with average grain sizes of the order of $\sim 1 \mu\text{m}$. It is important, therefore, to evaluate the influence of this fine grain structure on the high temperature mechanical properties of magnesium alloys at low stresses.

If the fine structure introduced by ECAP processing is stable at high temperatures, the material may undergo superplastic deformation which is controlled by grain boundary sliding [47]. In the present experiments, the high temperature mechanical prop-

erties of magnesium alloys were evaluated by tensile testing. This type of testing provides the flow stress as a function of the strain for different imposed strain rates. It is also possible to evaluate the material ductility by measuring the final elongation after specimen failure. As the material behavior depends strongly on the strain rate at high temperatures, different tensile tests are generally conducted at different strain rates for each testing temperature. It is also possible to vary the strain rate in a single tensile test to determine the strain rate sensitivity in the so-called jump-test. As the specimen geometry changes during tensile deformation, it is important to account for the effect of the reduction of the cross-sectional area in order to determine the true stress and true strain data.

An example of true stress-true strain curves are shown in Fig. 7 where these curves were determined by the tensile testing of an AZ31 magnesium alloy (Mg-3% Al-1% Zn) which was processed through 4 passes of ECAP [48]. The tests were carried out at different initial strain rates varying from $\sim 10^{-4}$ to $\sim 10^{-1} \text{ s}^{-1}$. The strain rate was also varied during the test by a factor of ~ 2 at the lower strain rates. It was observed that the material strength varied considerably depending on the strain rate. A yield stress of $\sim 20 \text{ MPa}$ was observed at the highest strain rate while a yield stress lower than $\sim 1 \text{ MPa}$ was observed at the slowest strain rate.

Fig. 8 shows the flow stress at a strain level of 0.1, normalized by the shear modulus, G , plotted as a function of the strain rate for the different testing temperatures [48]. The data are plotted in a logarithmic scale in order to ease the determination of the strain rate sensitivity, m , from the slope of the curve. This slope shows that the strain rate sensitivity is ~ 0.5 for the tested conditions and in practice a strain rate sensitivity in the range of $\sim 0.4 - 0.5$ is characteristic of the grain boundary sliding mechanism [46]. Strain rate sensitivities at this level were reported earlier for different magnesium alloys processed by ECAP and tested at high temperatures. For example, a coefficient of $m \approx 0.4$ was reported for a Mg-7.5% Al-0.2% Zr alloy [49], a similar value for m was reported in a ZK60 (Mg-5.5% Zn-0.5% Zr) alloy [50], values in the range of $m \approx 0.3 - 0.5$ were reported for an AZ91 (Mg-9% Al-1% Zn) alloy [51] and $m \approx 0.5$ was reported in a Mg-8% Li alloy [52]. Another way to evaluate the relationship between strain rate and stress is to plot the strain rate as a function of the stress and to determine the stress exponent. The stress exponents are the inverse of the coefficient m and thus a strain rate sensitivity of ~ 0.5 corresponds to a stress exponent of

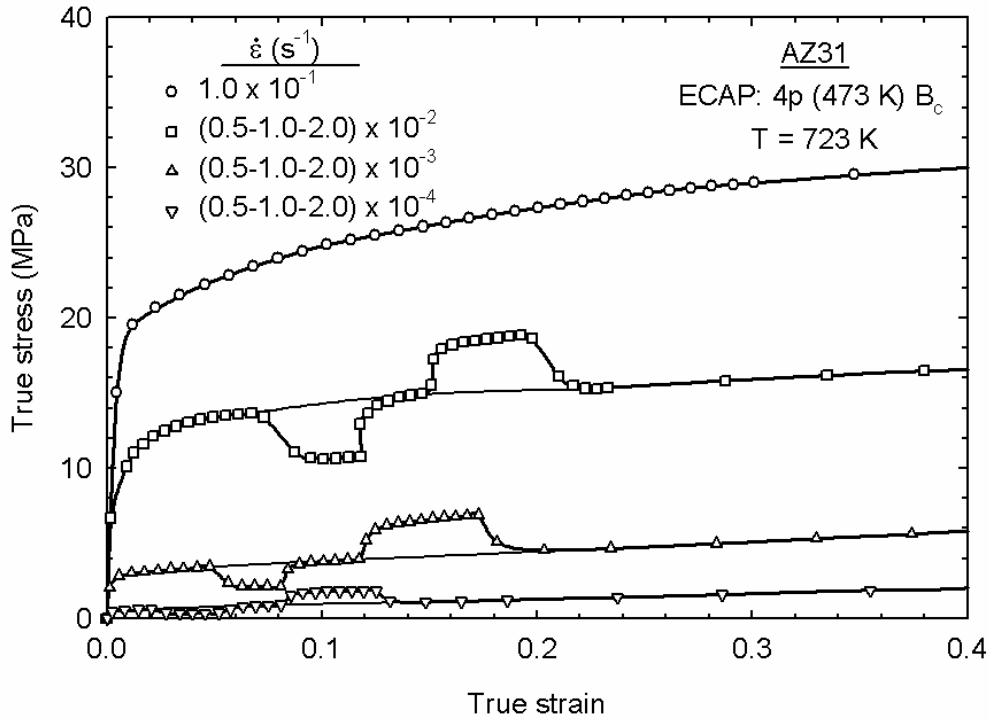


Fig. 7. True stress-true strain curves determined at different strain rates for the AZ31 alloy processed by 4 passes of ECAP (data from [48]).

$n \approx 2$ which is similar to the stress exponent in the relationship for superplastic flow shown in Eq. (3).

Fig. 9 shows the normalized strain rate, recorded at a normalized stress of $2 \cdot 10^{-4}$, as a function of the inverse of the testing temperature. The slope of the line leads to an activation energy, Q , of $\sim 84 \text{ kJ mol}^{-1}$ where this value is close to the activation energy for grain boundary diffusion in magnesium of $Q_{gb} \approx 92 \text{ kJ mol}^{-1}$ [39]. This type of diffusion is similar to that expected for superplastic flow as shown in Eq. (3). It should be noted that del Valle and Ruano [53] also reported an activation energy similar to the value for grain boundary diffusion in a fine-grained AM60 (Mg-6% Al-0.5% Mn) alloy tested at high temperatures and low stresses.

Thus, both the strain rate sensitivity and the activation energy for diffusion for different magnesium alloys are in agreement with the anticipated relationship for grain boundary sliding as the rate-controlling mechanism. In order to check the agreement with the theoretical model and the behavior of magnesium alloys processed by ECAP, several sets of data from experimental tests are compared to the prediction from Eq. (3) in Fig. 10 [48,50,53-55]. The strain rate was normalized by the effect of the

different testing temperatures and grain sizes by considering grain boundary diffusion and an inverse spatial grain size exponent of 2. The normalized strain rate is plotted as a function of the stress normalized by the shear modulus and the line for the theoretical prediction for the grain boundary sliding mechanism is also shown. It is observed that the experimental data for different magnesium alloys with different grain sizes tested at different temperatures agree with the theoretical prediction for grain boundary sliding where this prediction relates to conventional superplastic flow. The data points tend to deviate from the predicted line at the highest stresses because of the gradual transition into the region of dislocation creep equivalent to region III.

The analysis shows that the grain refinement produced by ECAP processing of magnesium alloys leads to the occurrence of grain boundary sliding at high temperatures. This deformation mechanism is therefore responsible for the occurrence of superplastic flow. The high strain rate sensitivity of ~ 0.5 leads to high elongations of the specimens which demonstrates directly the occurrence of superplasticity. Typically, elongations larger than 500% are attributed to superplasticity.

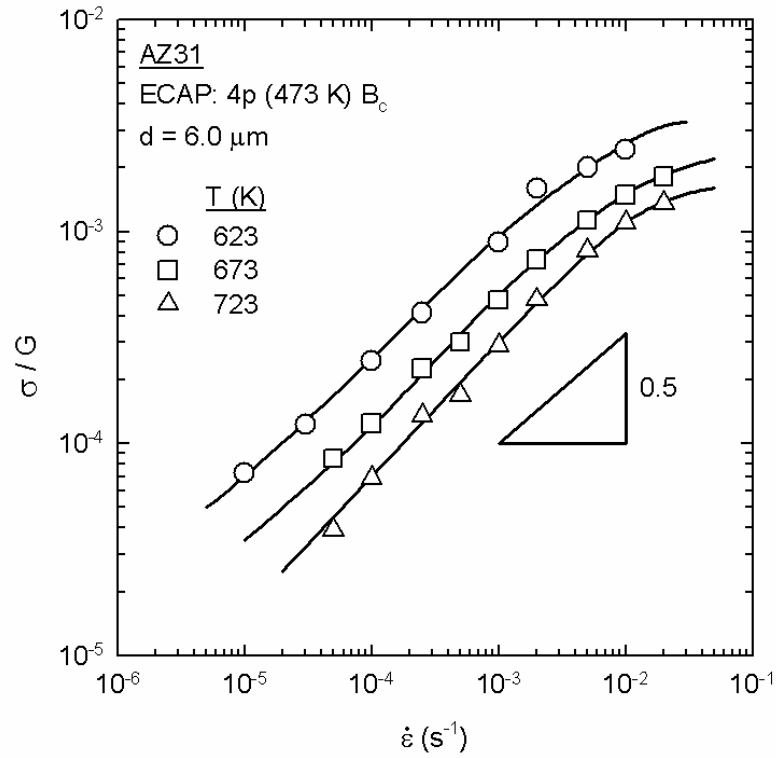


Fig. 8. Flow stress normalized by shear modulus as a function of strain rate for the AZ31 alloy processed by 4 passes of ECAP (data from [48]).

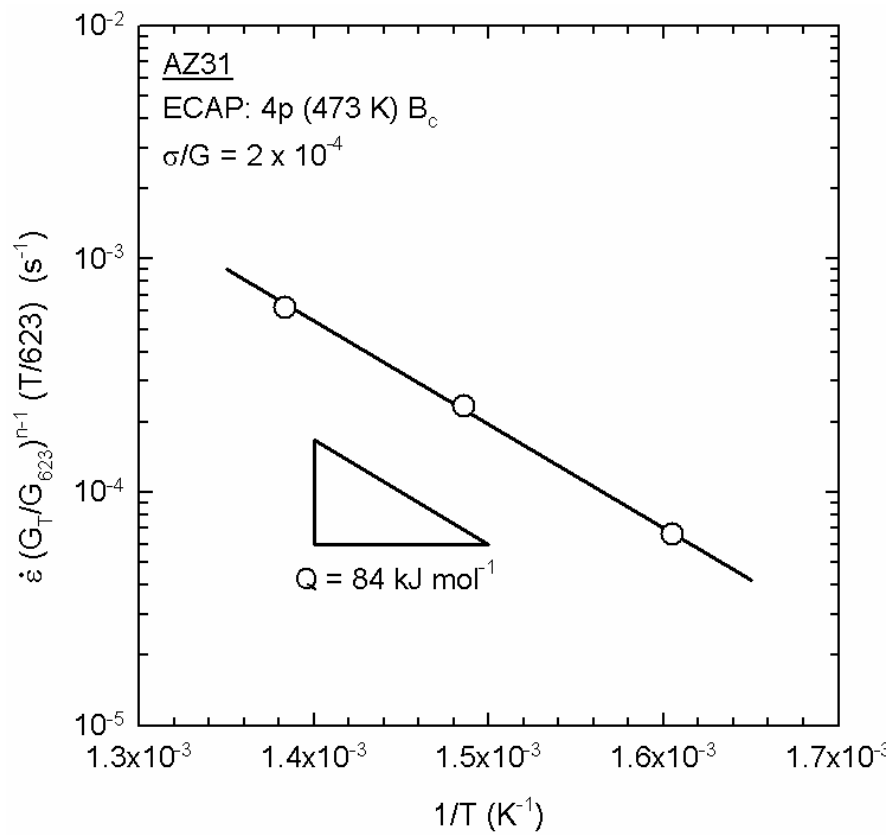


Fig. 9. Normalized strain rate for a normalized stress of $2.0 \cdot 10^{-4} \text{ s}^{-1}$ plotted as a function of the inverse of temperature for the AZ31 alloy (data from [48]).

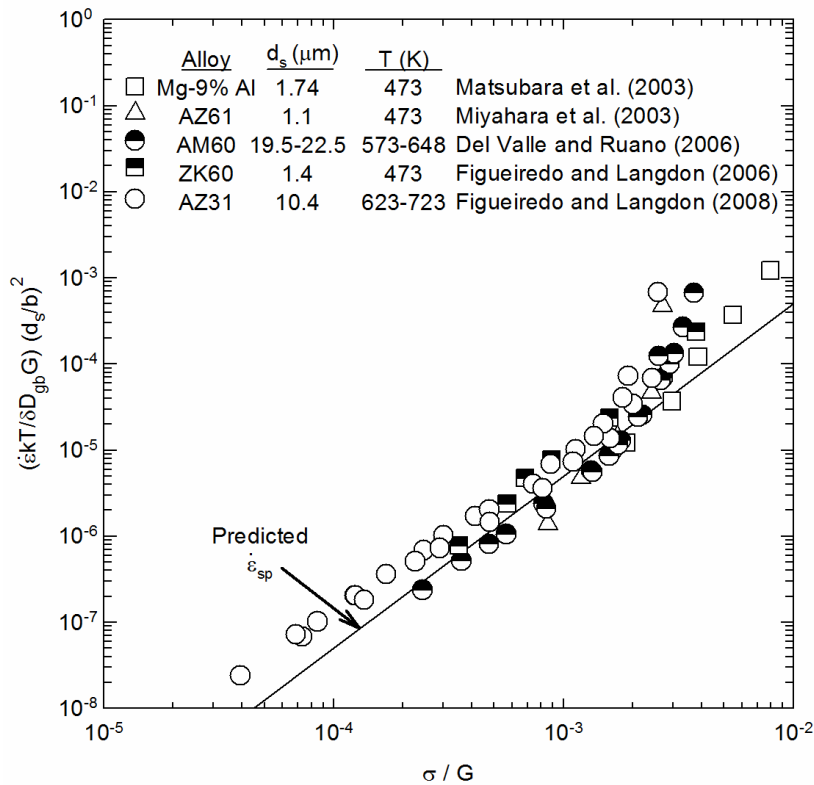


Fig. 10. Strain rate normalized by temperature and grain size plotted as a function of the flow stress normalized by the shear modulus for different magnesium alloys processed by ECAP (data from [48,50,53-55]); the solid line shows the prediction for superplastic flow (data from [46]).

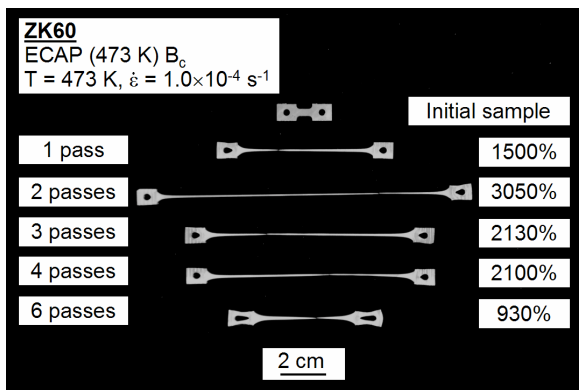


Fig. 11. Appearance of tensile specimens of a ZK60 alloy processed by different numbers of passes of ECAP and tested in tension at 473K with an initial strain rate of $1.0 \cdot 10^{-4} \text{ s}^{-1}$ (data from [58]).

[56,57]. This characteristic, allied to the pronounced grain refinement induced by ECAP processing, is expected to lead to very high ductilities. In fact, high elongations have been reported in different magnesium alloys processed by ECAP including an elongation of $\sim 1780\%$ in a Mg-8% Li alloy [52] and a record elongation of $\sim 3050\%$ in a ZK60 alloy [58]. Fig. 11 shows the appearance of specimens of this alloy after pulling to failure in tension at 473K with an initial strain rate of $1.0 \cdot 10^{-4} \text{ s}^{-1}$ [58]. These specimens were processed by different numbers of passes of ECAP before testing in tension and the elongations confirm that this processing parameter has a strong influence on the superplastic properties of the material.

5. SUMMARY AND CONCLUSIONS

1. The application of severe plastic deformation (SPD) to bulk solids leads to significant grain refinement to the submicrometer or even nanometer range. This opens the possibility of revealing dif-

The maximum elongation recorded during tensile superplasticity is usually limited by the development of internal cavities. However, magnesium alloys exhibit a high resistance to the development of cavities during low temperature superplasticity

ferent flow mechanisms when testing at elevated temperatures, including the advent of Nabarro-Herring and Coble diffusion creep and/or superplastic flow controlled by grain boundary sliding.

2. Tests on high-purity aluminum show it is not possible to reveal the occurrence of diffusion creep in creep testing because the ultrafine grains introduced by SPD are unstable at high temperatures. By contrast, excellent superplastic properties are attained in a two-phase Zn-22% Al alloy and in various magnesium alloys after processing by SPD.

ACKNOWLEDGEMENTS

One of the authors (RBF) was supported by a CAPES/Fulbright Scholarship. This work was supported by the U.S. Army Research Office under Grant No. W911NF-08-1-0201.

REFERENCES

- [1] R.Z. Valiev, R.K. Islamgaliev and T.G. Langdon // *Prog. Mater. Sci.* **45** (2000) 103.
- [2] R.Z. Valiev and T.G. Langdon // *Prog. Mater. Sci.* **51** (2006) 881.
- [3] A.P. Zhilyaev and T.G. Langdon // *Prog. Mater. Sci.* **53** (2008) 893.
- [4] R.Z. Valiev, Y. Estrin, Z. Horita, T.G. Langdon, M.J. Zehetbauer and Y.T. Zhu // *JOM* **58** (4) (2006) 33.
- [5] T.G. Langdon // *Metall. Trans. A* **13A** (1982) 689.
- [6] A.J. Barnes // *J. Mater. Eng. Perform.* **16** (2007) 440.
- [7] R.Z. Valiev, O.A. Kaibyshev, R.I. Kuznetsov, R.Sh. Musalimov and N.K. Tsenev // *Dokl. Akad. Nauk SSSR* **301** (1988) 864.
- [8] Z. Horita, M. Furukawa, M. Nemoto, A.J. Barnes and T.G. Langdon // *Acta Mater.* **48** (2000) 3633.
- [9] M. Kawasaki, R.B. Figueiredo, C. Xu and T.G. Langdon // *Metall. Mater. Trans. A* **38A** (2007) 1891.
- [10] R.B. Figueiredo, M. Kawasaki, C. Xu and T.G. Langdon // *Mater. Sci. Eng.* **A493** (2008) 104.
- [11] M. Furukawa, Y. Iwahashi, Z. Horita, M. Nemoto and T.G. Langdon // *Mater. Sci. Eng.* **A257** (1998) 328.
- [12] M. Furukawa, Z. Horita and T.G. Langdon // *Mater. Sci. Eng.* **A332** (2002) 75.
- [13] Y. Iwahashi, J. Wang, Z. Horita, M. Nemoto and T.G. Langdon // *Scripta Mater.* **35** (1996) 143.
- [14] Y. Iwahashi, Z. Horita, M. Nemoto and T.G. Langdon // *Acta Mater.* **45** (1997) 4733.
- [15] K. Nakashima, Z. Horita, M. Nemoto and T.G. Langdon // *Acta Mater.* **46** (1998) 1589.
- [16] Y. Iwahashi, Z. Horita, M. Nemoto and T.G. Langdon // *Acta Mater.* **46** (1998) 3317.
- [17] S.D. Terhune, D.L. Swisher, K. Oh-ishi, Z. Horita, T.G. Langdon and T.R. McNelley // *Metall. Mater. Trans. A* **33A** (2002) 2173.
- [18] M. Kawasaki, I.J. Beyerlein, S.C. Vogel and T.G. Langdon // *Acta Mater.* **56** (2008) 2307.
- [19] V. Sklenicka, J. Dvorak and M. Svoboda, In: *Nanomaterials by Severe Plastic Deformation (NanoSPD2)*, ed. by M.J. Zehetbauer and R.Z. Valiev (Wiley-VCH: Weinheim, Germany, 2002), p. 200.
- [20] V. Sklenička, J. Dvořák and M. Svoboda // *Mater. Sci. Eng.* **A387-389** (2004) 696.
- [21] V. Sklenicka, J. Dvorak and M. Svoboda, In: *Ultrafine Grained Materials III*, ed. by Y.T. Zhu, T.G. Langdon, R.Z. Valiev, S.L. Semiatin, D.H. Shin and T.C. Lowe (The Minerals, Metals and Materials Society: Warrendale, PA, 2004), p. 647.
- [22] V. Sklenička, J. Dvořák, P. Kral, Z. Stonawska and M. Svoboda // *Mater. Sci. Eng.* **A410-411** (2005) 408.
- [23] V. Sklenička, J. Dvořák, M. Kvapilova, M. Svoboda, P. Král, I. Saxl and Z. Horita // *Mater. Sci. Forum* **539-543** (2007) 2904.
- [24] P. Král, J. Dvořák and V. Sklenička // *Mater. Sci. Forum* **584-586** (2008) 846.
- [25] Y.J. Li, X.H. Zeng and W. Blum // *Acta Mater.* **52** (2004) 5009.
- [26] W. Blum and Y.J. Li // *Phys. Stat. Sol. (a)* **201** (2004) 2915.
- [27] W. Blum and Y.J. Li, In: *Creep Deformation and Fracture Design, and Life Extension*, ed. by R.S. Mishra, J.C. Earthman, S.V. Raj and R. Viswanathan (The Minerals, Metals and Materials Society: Warrendale, PA, 2005), p. 65.
- [28] Y.J. Li, R. Valiev and W. Blum // *Mater. Sci. Eng.* **A410-411** (2005) 451.
- [29] T.G. Langdon // *Scripta Metall.* **4** (1970) 693.
- [30] J. Wang, Z. Horita, M. Furukawa, M. Nemoto, N.K. Tsenev, R.Z. Valiev, Y. Ma and T.G. Langdon // *J. Mater. Res.* **8** (1993) 2810.
- [31] J. Wang, Y. Iwahashi, Z. Horita, M. Furukawa, M. Nemoto, R.Z. Valiev and T.G. Langdon // *Acta Mater.* **44** (1996) 2973.

- [32] Z. Horita, D.J. Smith, M. Furukawa, M. Nemoto, R.Z. Valiev and T.G. Langdon // *J. Mater. Res.* **11** (1996) 1880.
- [33] T.G. Langdon // *Z. Metallkd.* **96** (2005) 522.
- [34] T.G. Langdon // *Mater. Trans.* **46** (2005) 1951.
- [35] F.R.N. Nabarro, *Report of a Conference on Strength of Solids* (The Physical Society: London, UK, 1948).
- [36] C. Herring // *J. Appl. Phys.* **21** (1950) 437.
- [37] R.L. Coble // *J. Appl. Phys.* **34** (1963) 1679.
- [38] F.A. Mohamed and T.G. Langdon // *Metall. Trans.* **5** (1974) 2339.
- [39] H.J. Frost and M.F. Ashby, *Deformation-Mechanism Maps; The Plasticity and Creep of Metals and Ceramics* (Pergamon Press: Oxford, UK, 1982).
- [40] T.G. Langdon // *Mater. Sci. Eng.* **A137** (1991) 1.
- [41] H. Ishikawa, F.A. Mohamed and T.G. Langdon // *Phil. Mag.* **32** (1975) 1269.
- [42] M. Kawasaki and T.G. Langdon // *Mater. Trans.* **49** (2008) 84.
- [43] M. Kawasaki and T.G. Langdon // *Mater. Sci. Eng. A* (2009), in press.
- [44] P. Kumar, C. Xu and T.G. Langdon // *Mater. Sci. Eng.* **A429** (2006) 324.
- [45] P. Kumar, C. Xu and T.G. Langdon // *Mater. Sci. Eng.* **A410-411** (2005) 447.
- [46] T.G. Langdon // *Acta Metall. Mater.* **42** (1994) 2437.
- [47] T.G. Langdon // *Mater. Sci. Eng.* **A174** (1994) 225.
- [48] R.B. Figueiredo and T.G. Langdon // *J. Mater. Sci.* **43** (2008) 7366.
- [49] Y. Miyahara, K. Matsubara, Z. Horita and T.G. Langdon // *Metall. Mater. Trans. A* **36A** (2005) 1705.
- [50] R.B. Figueiredo and T.G. Langdon // *Mater. Sci. Eng.* **A430** (2006) 151.
- [51] M. Mabuchi, K. Ameyama, H. Iwasaki and K. Higashi // *Acta Mater.* **47** (1999) 2047.
- [52] M. Furui, H. Kitamura, H. Anada and T.G. Langdon // *Acta Mater.* **55** (2007) 1083.
- [53] J.A. del Valle and O.A. Ruano // *Acta Mater.* **55** (2007) 455.
- [54] Y. Miyahara, Z. Horita and T.G. Langdon // *Mater. Sci. Eng.* **A420** (2006) 240.
- [55] K. Matsubara, Y. Miyahara, Z. Horita and T.G. Langdon // *Acta Mater.* **51** (2003) 3073.
- [56] C.J. Lee and J.C. Huang // *Acta Mater.* **52** (2004) 3111.
- [57] A. Mussi, J.J. Blandin, L. Salvo and E.F. Rauch // *Acta Mater.* **54** (2006) 3801.
- [58] R.B. Figueiredo and T.G. Langdon // *Adv. Eng. Mater.* **10** (2008) 37.